PCCP

PAPER

View Article Online
View Journal | View Issue

Cite this: *Phys. Chem. Chem. Phys.*, 2016, **18**, 33109

Received 14th September 2016,
Accepted 15th November 2016

DOI: 10.1039/c6cp06323c

www.rsc.org/pccp

High-pressure dielectric behavior of $BaMoO_4$: a combined experimental and theoretical study†

Tianru Qin,[a] Qinglin Wang,[b] Li Wang,[a] Huacai Yan,[a] Cailong Liu,[a] Yonghao Han,[a] Yanzhang Ma[cd] and Chunxiao Gao*[a]

In situ impedance measurements were employed to investigate the electrical transport properties of $BaMoO_4$ under pressures of up to 20.0 GPa. Two anomalous changes in the electrical parameters were found, related to the pressure-induced structural phase transitions. The dielectric performance of $BaMoO_4$ was improved by pressure. The dispersion in the real part of dielectric constant *versus* frequency weakens with increasing pressure. Based on the first-principles calculations, the increases of resistance with increasing pressure in the tetragonal and monoclinic phases were mainly caused by the increasing defect levels. The decrease of the relative permittivity in the tetragonal phase was attributed to pressure-induced strengthening in electronic localization around Mo atoms, which hindered the polarization of Mo–O electric dipoles.

1. Introduction

Alkaline molybdate materials with the chemical formula $AMoO_4$ (A = Ca, Sr, Ba), in which the A atom has eightfold oxygen coordination and the molybdate atom forms a MoO_4^{2-} tetrahedron, have captured much attention due to their promising application prospects, such as in scintillators and solid-state lasers. These materials are also possible candidates for microwave dielectric devices with their low dielectric constant and high-quality factor.[1–7] Barium molybdate, as a member of this family with its outstanding luminous characteristic, has eminent performance in the electro-optical field.[8–11] The application of these materials is established on the basis of their excellent electrical and dielectric properties. Various synthesis methods have been reported to obtain the scheelite-type $BaMoO_4$ compound, such as hydrothermal route, solid-state reaction, and co-precipitation.[2,8,12] Generally, the synthesis processes cause unevenly distributed stress/strain in the crystal, such as the distorted/fractured chemical bond and generated dangling bond in the crystal, which leads to changes in the ions' environment. In addition, the impurity-induced, unevenly distributed charges also result in distorted crystal structure and consequently change the properties of materials. For example, the luminescence properties of $BaMoO_4$ are greatly dependent on the morphologies and sizes, which are determined by synthesis conditions, such as reaction temperature and chemical composition.[13–15] These research studies are beneficial for understanding the role of the impurities and crystallization integrity, but cannot reveal the effect of the stress/strain. Therefore, a detailed investigation of the pressure-tuned dielectric properties is essential.

The structural stability of $BaMoO_4$ under compression has been studied previously. Christofilos *et al.* found a reversible structural transition at 5.8 GPa by Raman spectroscopy at up to 8 GPa.[16] Using Raman and X-ray diffraction experiments, combined with the GSAS software, Panchal *et al.* extended the pressure up to 13.0 GPa and uncovered that $BaMoO_4$ experienced two phase transitions from the initial tetragonal structure to the monoclinic and the unknown structures at 5.8 and 7.2 GPa, respectively.[17] However, high-pressure studies on $BaMoO_4$ are still not comprehensive—the electrical transport properties of $BaMoO_4$ under compression were scarcely tackled, despite its significant importance for fundamental physics, thus limiting the optimization of $BaMoO_4$-based applications. Compression not only can drive materials toward higher-density structures and consequently tune the intra- and intermolecular structures, but it also can tune the electrical transport properties of materials.[18,19] It is still uncertain how pressure affects the electrical transport properties of $BaMoO_4$, such as the carrier scattering, the relaxation process and the complex dielectric properties, and this motivated us to explore the high-pressure electrical transport properties of $BaMoO_4$.

[a] *State Key Laboratory of Superhard Materials, Jilin University, Changchun 130012, China. E-mail: cc060109@qq.com*
[b] *Shandong Key Laboratory of Optical Communication Science and Technology, School of Physics Science & Information Technology of Liaocheng University, Liaocheng 252059, China*
[c] *Department of Mechanical Engineering, Texas Tech University, Lubbock, Texas 79409, USA*
[d] *Center for High Pressure Science & Technology Advanced Research, Changchun 130012, China*

† Electronic supplementary information (ESI) available: X-ray diffraction pattern of the $BaMoO_4$ sample, further details about dE_g/dP obtained theoretically and $d(\ln R)/dP$ obtained experimentally. See DOI: 10.1039/c6cp06323c

In this work, we conducted a comprehensive investigation on the high-pressure electrical transport properties of polycrystalline $BaMoO_4$ by using *in situ* alternate-current (AC) impedance spectra measurements in a diamond anvil cell (DAC) at up to 20.0 GPa. In addition to the variation of resistance, frequency and relative dielectric constant with pressure, the complex permittivity, modulus and dielectric loss of $BaMoO_4$ under high pressure were also discussed in this paper. Meanwhile, first-principles calculations were employed to gain a better understanding of the electrical transport behavior of $BaMoO_4$ under compression.

2. Experimental section

$BaMoO_4$ powder with purity of 99.9% was purchased from the Alfa Aesar Co. The initial structure of the sample was tetragonal (S.G. $I4_1/a$), which has been confirmed by X-ray diffraction measurement (ESI†). High-pressure experiments were conducted by using a diamond anvil cell (DAC) with the anvil culet of 300 μm in diameter. The impedance spectroscopy was measured with parallel-plate electrodes. The fabrication process of the detecting microcircuit on two diamond anvils has been reported in our previous works.[20–22] A ruby fluorescence method was used for pressure calibration.[23] The applied pressure was calibrated by observing the pressure-induced shift of the sharp fluorescent R1 ruby line. No pressure medium was loaded, in order to avoid introducing impurities for measurement of electrical parameters and to ensure good electrical contact.

The impedance measurements were conducted by using a Solartron 1260 impedance analyzer equipped with Solartron 1296 dielectric interface. A 1.0 V sine signal was applied to the sample with a frequency ranging from 10^{-3} Hz to 10^6 Hz. The pressure was up to 20.0 GPa. The testing environment was controlled and kept stable during all the measurements.

The first-principles calculations were performed on the basis of the density functional theory (DFT) and pseudo potential method.[24] All of the calculations were carried out by the CASTEP code.[25] The electron–ion interaction was described by Vanderbilt-type ultrasoft pseudo potentials.[26] The exchange and correlation terms were described with generalized gradient approximations (GGA) in the scheme of Perdew–Burke–Ernzerhof (PBE).[27] The unit cell was optimized by the Broyden–Fletcher–Goldfarb–Shanno (BFGS) minimization algorithm provided in the CASTEP code. Integration in the Brillouin zone was performed using special k points generated with $6 \times 6 \times 8$ and $7 \times 7 \times 8$ mesh parameter grids for the tetragonal and monoclinic phase. The one-electron valence state was expanded on the basis of plane wave with the cut-off energy of 340 eV.

3. Results and discussion

The complex plane impedance spectra of $BaMoO_4$ under various pressures are shown in Fig. 1(a). Under compression, the effect of interface between the grains on the crystal's properties is determined by the response of the grain boundary to the variable-frequency electrical signal. However, only one semicircle

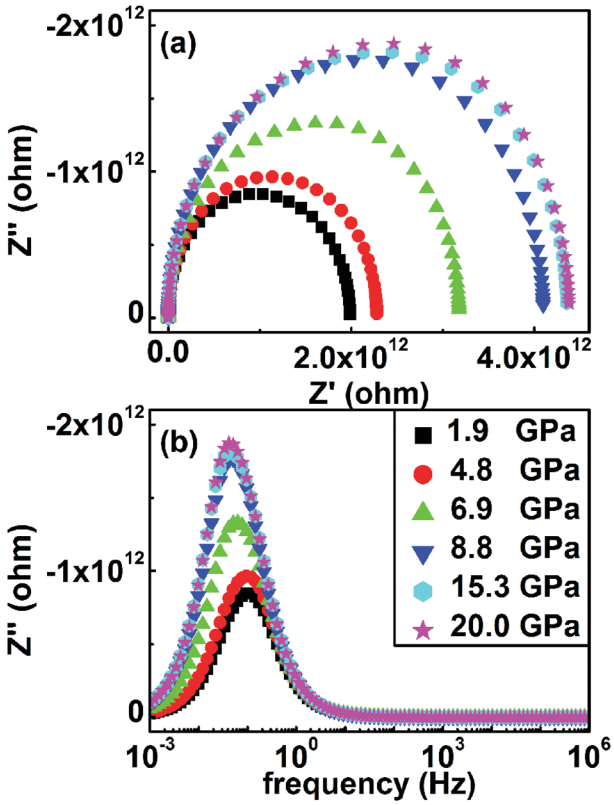

Fig. 1 (a) The impedance spectra Z'–Z'' and (b) the frequency dependence of imaginary part under compression.

existed in our measurement results, which represents the transport property of the grains. The grain boundary did not have a significant impact on the properties of $BaMoO_4$ under compression, which is a valuable result for its practical application. Therefore, $BaMoO_4$ can be regarded as a typical material for studying the crystal interior features. The frequency dependence of imaginary part Z'' under different pressures is displayed in Fig. 1(b). The width of the relaxation peak broadens with increasing pressure, indicating that the pressure-dependent relaxation process does exist in $BaMoO_4$. The relaxation peaks shift to the low-frequency part with increasing pressure.

According to the Z'-intercept in Fig. 1(a), we can acquire the resistance (R) at different pressures, as shown in Fig. 2(a). According to the variable relationship between frequency and Z'' in Fig. 1(b), the relaxation frequency *versus* pressure can be deduced as shown in Fig. 2(b). Two discontinuous changes were found at 4.8 GPa and 8.8 GPa, respectively, which were related to the pressure-induced structural phase transitions.[17] Generally, the non-hydrostatic pressure can produce deviatoric stresses in the sample, thus influencing the pressure-driven transitions, including the phase transition pressure or the phase transition sequence.[28–30] In our experiments, the phase transition sequence is not affected by the deviatoric stresses. The different transition pressures between our work and ref. 17 can be attributed to the non-hydrostatic effect, which indicates that the deviatoric stresses result in obvious transition pressure drop in $BaMoO_4$. The transport characteristics of the electrons

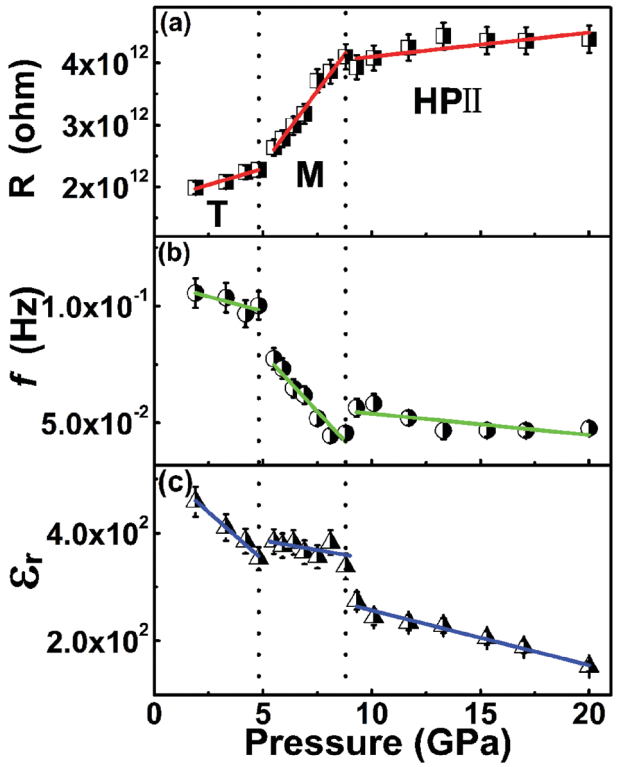

Fig. 2 (a) Pressure dependence of $BaMoO_4$ resistance. (b) Variation of the relaxation frequency with pressure. (c) Variation of the relative permittivity of $BaMoO_4$ with pressure. T, M, and HP-II represent the tetragonal phase, the monoclinic phase and the unknown high-pressure phase, respectively.

depend on the lattice scattering and the defect density. The increase of R with increasing pressure may be for two reasons: the carrier concentration is constant, and defect levels increase, leading to an enhanced lattice scattering effect; the defect levels keep constant, and the carrier concentration decreases due to the band gap widening. We will discuss this point in the first-principles calculations part.

From 1.9 GPa to 4.8 GPa, the frequency decreases slowly with increasing pressure. However, in the pressure range from 4.8 GPa to 8.8 GPa, the frequency shows an obvious downward trend, which can be explained as follows: during the structural phase transition, additional energy barriers were generated due to the effect of pressure. The charge carrier transport through grains becomes more difficult, leading to longer relaxation time. In addition, the increasing of defect varieties, dangling bonds and the crystal structural disorder can also result in a decreasing trend in relaxation frequency. Above 8.8 GPa, the relaxation frequency of the unknown high-pressure phase decreases smoothly up to 20.0 GPa. In addition, the activation energy and the dielectric properties of $BaMoO_4$ can be obtained. In fact, the relaxation frequency denotes the charge–discharge rate of the dipole oscillation process, and the activation energy represents the energy to activate the resonance.[31] The relationship between the relaxation frequency and the activation energy can be expressed according to the Arrhenius equation,

$$f = f_0 \exp(-E/k_B T), \quad (1)$$

Table 1 The pressure dependence of activation energy

Phase	Pressure region (GPa)	dE/dP (meV GPa^{-1})
Tetragonal	1.9–4.8	0.63
Monoclinic	4.8–8.8	4.65
HPII	8.8–20.0	0.48

where E represents the activation energy, k_B is the Boltzmann constant, and T is the temperature. Supposing that f and E are only functions of pressure, and f_0 remains constant, we can obtain the following relationship by calculating the first-order derivative on pressure.

$$d(\ln f)/dP = -(1/k_B T)(dE/dP), \quad (2)$$

By linear fitting to the curve of $\ln f \sim P$, we acquired the pressure dependence of the activation energy (dE/dP) shown in Table 1. In the entire pressure range, the activation energy shows a positive correlation with pressure, indicating that the charge–discharge process becomes more difficult and the vibration damping of Mo–O dipoles is strengthened with increasing pressure.

The relative dielectric constant of $BaMoO_4$ under compression can be obtained based on the following relationship:

$$\varepsilon_r(P) = d/(2\pi R \varepsilon_0 f S), \quad (3)$$

where d is the thickness of the sample, ε_0 is the vacuum permittivity, S is the area of electrode, and f is the relaxation frequency. Fig. 2(c) shows the pressure dependence of ε_r up to 20.0 GPa. The ε_r decreases obviously with increasing pressure in the tetragonal and HPII phases, but decreases relatively slowly in the monoclinic phase. With pressure increasing, the grain size reduced progressively, resulting in a shorter distance within which the electric dipoles align in phase, and the total dipole moment becomes smaller. The smaller grains can store less energy during realignment with transmitted electric field, leading to a decreasing trend of ε_r and capacitance with increasing pressure. In addition, the state of the electron localization around atoms also is related to ε_r; we will come back to this point later.

To gain a comprehensive understanding of the electrical properties of $BaMoO_4$, the dielectric properties were further studied. The complex permittivity (ε', ε'') and the dielectric loss tangent ($\tan\delta$) with frequency under various pressures are shown in Fig. 3. A monodispersive nature of dielectric relaxation was found. The ε' decrease with increasing frequency below 1 Hz can be explained by the decreasing number of dipoles that contribute to polarization. The ε' keeps a constant value when the frequency is higher than 1 Hz, which can be attributed to the rapid polarization processes occurring in $BaMoO_4$ under the induced field. In addition, the dispersion in ε' *versus* f weakens with increasing pressure. The ε'' is reduced with increasing frequency, indicating that the energy loss was caused by the electron conduction.

The value of $\tan\delta$ is the ratio of the energy dissipated in the material to the energy stored over a period of time, and it determines the mechanism of the ac conduction and dielectric relaxation. The $\tan\delta$ increases as the frequency decreases and reaches the maximum value at 10^{-3} Hz. At 10^{-3} Hz, as shown in

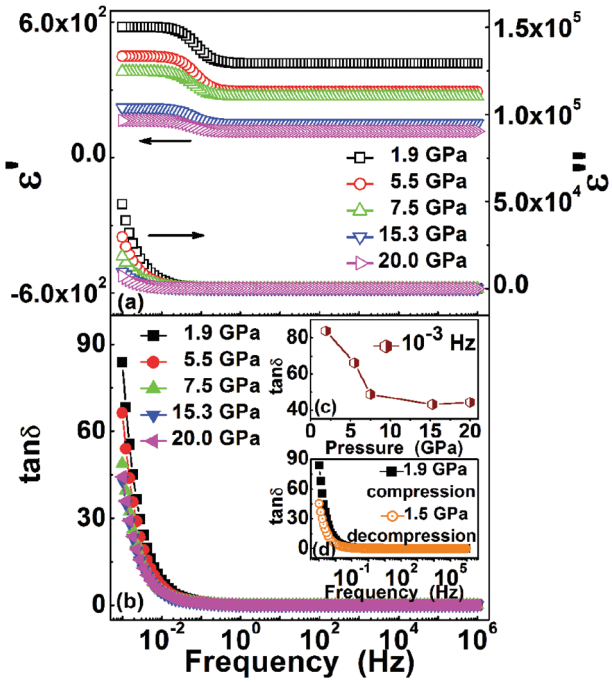

Fig. 3 (a) Variation of the complex permittivity of $BaMoO_4$ with pressure. (b) Dielectric loss factor ($\tan\delta$) *versus* frequency of $BaMoO_4$ at a few representative pressures. Inset: (c) Loss tangent *versus* pressure at a low frequency of 10^{-3} Hz. (d) Loss tangent at 1.9 GPa and 1.5 GPa after pressure release.

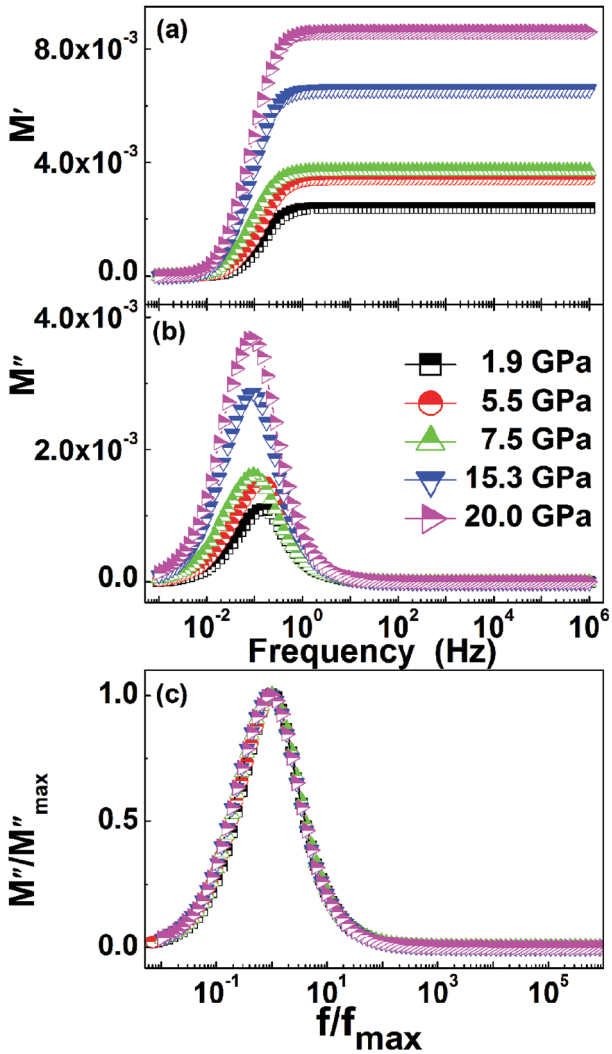

Fig. 4 Frequency dependence of (a) M' and (b) M'' at different pressures. (c) Variation of M''/M_{max}'' with f/f_{max} at different pressures of $BaMoO_4$.

the inset (c) of Fig. 3, the value of $\tan\delta$ presents a significant downward trend with the increasing pressure, which is decreased from 83 to 44. When pressure is released to 1.5 GPa, as shown in the inset (d) of Fig. 3, the maximum value at 10^{-3} Hz is much lower than the initial state, and the range of loss frequency becomes narrow, which indicates that the crystal microstructure (*i.e.*, grain size and orientation) rearranges after a pressure cycle, and the dielectric properties have been changed.

Generally, the changes of thermodynamic conditions in the application of materials, the stress/strain will be produced, and the situation of chemical/dangling bonds within the crystals will be changed. Compression can produce extreme stress/strain conditions, which makes it very effective in studying the stress/strain effects on properties of materials. Our research indicates that the dielectric loss has been decreased significantly after decompression, suggesting that the dielectric performance of $BaMoO_4$ is improved by pressure.

The usage of complex modulus plots M^* ($M^* = j\omega C_0 Z^*$) is particularly useful to understand the electrical behavior, since the Z'' plots highlight phenomena characterized by the large resistance, whereas M'' plots identify electrical responses with small capacitance.[32] The complex electric modulus as a function of frequency at different pressures is shown in Fig. 4(a) and (b). Combining impedance Z'' and modulus M'' spectroscopic plots against frequency is an effective method for analyzing ac impedance data. Fig. 1(b) and 4(b) show a single peak in each plot, indicating that only one electrical response mechanism exists in $BaMoO_4$. The value of M' was found to be nearly zero in the low-frequency region but increased in the dispersion upon increasing frequency, with a tendency to saturate at a maximum asymptotic value in the high-frequency region for all the pressures. This is due to a lack of restoring force to control the mobility of the charge carriers with the induced electric field. In the frequency range of this transition, peaks in the values of M'' are developed, which shift to the lower-frequency part with increasing pressure, supporting the relaxation process. This indicates that the relaxation rate for this process decreases with increasing pressure. The M''/M_{max}'' against f/f_{max} at different pressures is plotted in Fig. 4(c). All these curves collapsed into one master curve, indicating that the dynamic processes in $BaMoO_4$ are pressure-independent. The frequency region where the peak occurs indicates the transition from long-range to short-range mobility on increasing frequency.

To better understand the electrical transport properties of $BaMoO_4$, we conducted the first-principles band structure and the charge density difference calculations below 8 GPa. Because the HPII phase is unknown, the calculation for this phase was

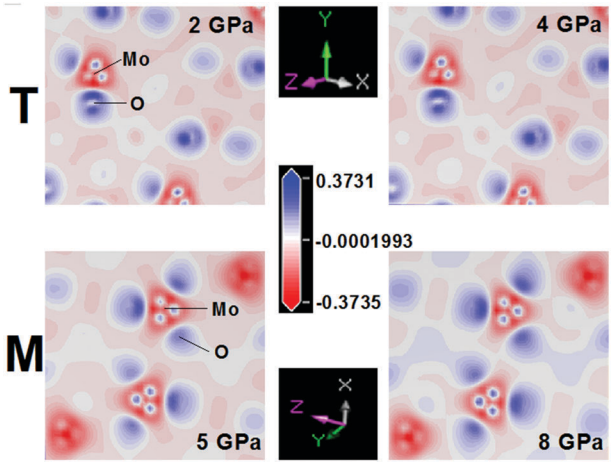

Fig. 5 Calculated charge density difference maps through the Mo and O atoms with an isosurface value of 0.1 for the tetragonal (T) phase (2, 4 GPa) and the monoclinic (M) phase (5, 8 GPa), respectively.

not conducted. The energy band structures of the tetragonal and monoclinic phases were calculated at different pressures. The variation rates of band gap (E_g) along with pressure were 1.2 meV GPa^{-1} and 0.4 meV GPa^{-1}, respectively. In addition, $d(\ln R)/d(P)$ obtained from the experiment are 0.05 GPa^{-1} and 0.14 GPa^{-1}, respectively. We compared dE_g/dP with $d(\ln R)/d(P)$ in the tetragonal and monoclinic phases and found that they do not satisfy the Arrhenius relationship; further detailed information about this is provided in the ESI.† Therefore, we concluded that the increase of R with pressure is mainly caused by the increasing defect levels, and the lattice scattering was enhanced. It is noted that the theoretically calculated E_g is valid only for intrinsic semiconductors. The estimate for the pressure-dependent band gap and the resistance is based on the intrinsic semiconductor hypothesis; the behavior of E_g in extrinsic semiconductors will be different than determined here.[33] In addition, previous research has indicated that the monoclinic phase has a reduced bond length (Mo–O and Ba–O) and is a denser phase compared with the tetragonal phase,[17] which will enhance the interaction force between atoms in the crystal and increase the activation energy. As a consequence, the carrier transportation becomes more difficult in the bulk, which can also lead to resistance increasing in monoclinic phase. The charge density difference maps at different pressures are shown in Fig. 5. As pressure increases, charge transfer occurs from O^{2-} ion to Mo^{6+} ion in the tetragonal phase. Thus, the decrease of the relative dielectric constant with pressure is caused by the enhancement of the electron localization around Mo atoms, and the polarization of Mo–O dipoles becomes more difficult. In the monoclinic phase, the charge transfer is less obvious, corresponding to the slowly downward trend of ε_r.

4. Conclusions

To summarize, we investigated the *in situ* high-pressure dielectric behavior of $BaMoO_4$ at up to 20.0 GPa. Pressure not only causes the structural phase transitions of $BaMoO_4$, but also changes its dielectric properties correspondingly. The increased activation energy indicates that the charge–discharge process becomes more difficult with increasing pressure. The increases in resistance with increasing pressure in the tetragonal and monoclinic phases were caused by the increasing defect levels. The obvious decrease of relative dielectric constant with pressure in the tetragonal phase is attributed to the enhanced electronic localization around Mo atoms. The dielectric loss at low frequency decreases significantly after a pressure cycle, suggesting that the dielectric performance of $BaMoO_4$ can be improved by pressure. The results of our work could provide useful guidance and help in some potential applications of $BaMoO_4$ and related ABO_4 materials.

Acknowledgements

This work was supported by the National Natural Science Foundation of China (Grant No. 11374121, 11404133, 11304034 and 11604133), the Program of Science and Technology Development Plan of Jilin Province (Grant No. 20140520105JH), the Open Project of State Key Laboratory of Superhard Materials (Jilin University, Grant No. 201612), and the Initial Foundation for Doctor Programme of Liaocheng University (Grant No. 318051610).

References

1 T. Thongtem, A. Phuruangrat and S. Thongtem, *Mater. Lett.*, 2008, **62**, 454–457.
2 B. K. Maji, H. Jena, R. Asuvathraman and K. V. G. Kutty, *J. Alloys Compd.*, 2015, **640**, 475–479.
3 Q. Gong, X. Qian, X. Ma and Z. Zhu, *Cryst. Growth Des.*, 2006, **6**, 1821–1825.
4 G.-K. Choi, J.-R. Kim, S. H. Yoon and K. S. Hong, *J. Eur. Ceram. Soc.*, 2007, **27**, 3063–3067.
5 J. H. Ryu, J.-W. Yoon, C. S. Lim, W.-C. Oh and K. B. Shim, *J. Alloys Compd.*, 2005, **390**, 245–249.
6 W.-S. Cho and M. Yoshimura, *Solid State Ionics*, 1997, **100**, 143–147.
7 D. Errandonea and F. J. Manjón, *Prog. Mater. Sci.*, 2008, **53**, 711–773.
8 Y.-S. Luo, W.-D. Zhang, X.-J. Dai, Y. Yang and S.-Y. Fu, *J. Phys. Chem. C*, 2009, **113**, 4856–4861.
9 J. H. Ryu, B. G. Choi, S. H. Kim, J.-W. Yoon, C. S. Lim and K. B. Shim, *J. Mater. Sci.*, 2005, **40**, 4979–4982.
10 A. P. A. Marques, D. M. A. de Melo, E. Longo, C. A. Paskocimas, P. S. Pizani and E. R. Leite, *J. Solid State Chem.*, 2005, **178**, 2346–2353.
11 C. Cui, J. Bi, F. Shi, X. Lai and D. Gao, *Mater. Lett.*, 2007, **61**, 4525–4527.
12 X. Zhao, T. L. Y. Cheung, Y. Xi, K. C. Chung, D. H. L. Ng and J. Yu, *J. Mater. Sci.*, 2007, **42**, 6716–6719.
13 M. Li, Y. Guan, Y. Yin, X. Cui, S. Rong, G. Jin, Y. Hao and Q. Wu, *Superlattices Microstruct.*, 2015, **80**, 222–228.
14 L. Ma, Y. Sun, P. Gao, Y. Yin, Z. Qin and B. Zhou, *Mater. Lett.*, 2010, **64**, 1235–1237.
15 Z. Luo, H. Li, H. Shu, K. Wang, J. Xia and Y. Yan, *Cryst. Growth Des.*, 2008, **8**, 2275–2281.

16 D. Christofilos, J. Arvanitidis, E. Kampasakali, K. Papagelis, S. Ves and G. A. Kourouklis, *Phys. Status Solidi B*, 2004, **241**, 3155–3160.
17 V. Panchal, N. Garg and S. M. Sharma, *J. Phys.: Condens. Matter*, 2006, **18**, 3917–3929.
18 L. Wang, F. Ke, Q. Wang, J. Yan, C. Liu, X. Liu, Y. Li, Y. Han, Y. Ma and C. Gao, *Appl. Phys. Lett.*, 2015, **107**, 201603.
19 J. Yan, F. Ke, C. Liu, Q. Wang, J. Zhang, L. Wang, G. Peng, Y. Han, Y. Ma and C. Gao, *Phys. Chem. Chem. Phys.*, 2015, **17**, 26277–26282.
20 C. He, C. Gao, Y. Ma, M. Li, A. Hao, X. Huang, B. Liu, D. Zhang, C. Yu, G. Zou, Y. Li, H. Li, X. Li and J. Liu, *Appl. Phys. Lett.*, 2007, **91**, 092124.
21 Y. Han, C. Gao, Y. Ma, H. Liu, Y. Pan, J. Luo, M. Li, C. He, X. Huang, G. Zou, Y. Li, X. Li and J. Liu, *Appl. Phys. Lett.*, 2005, **86**, 064104.
22 Q. Wang, C. Liu, Y. Gao, Y. Ma, Y. Han and C. Gao, *Appl. Phys. Lett.*, 2015, **106**, 132902.
23 G. J. Piermarini, S. Block, J. D. Barnett and R. A. Forman, *J. Appl. Phys.*, 1975, **46**, 2774.
24 S. Baroni, P. Giannozzi and A. Testa, *Phys. Rev. Lett.*, 1987, **58**, 1861–1864.
25 T. H. Fischer and J. Almlof, *J. Phys. Chem.*, 1992, **96**, 9768–9774.
26 D. Vanderbilt, *Phys. Rev. B: Condens. Matter Mater. Phys.*, 1990, **41**, 7892–7895.
27 J. P. Perdew, K. Burke and M. Ernzerhof, *Phys. Rev. Lett.*, 1996, **77**, 3865.
28 D. Errandonea, L. Gracia, R. Lacomba-Perales, A. Polian and J. C. Chervin, *J. Appl. Phys.*, 2013, **113**, 123510.
29 B. Liu, R. Liu, Q.-J. Li, M.-G. Yao, B. Zou, T. Cui, B.-B. Liu and J. Liu, *Chin. Phys. C*, 2013, **37**, 098003.
30 D. Errandonea, A. Muñoz and J. Gonzalez-Platas, *J. Appl. Phys.*, 2014, **115**, 216101.
31 Q. Wang, Y. Han, C. Liu, Y. Ma, W. Ren and C. Gao, *Appl. Phys. Lett.*, 2012, **100**, 172905.
32 D. C. Sinclair and A. R. West, *J. Appl. Phys.*, 1989, **66**, 3850.
33 D. Errandonea, E. Bandiello, A. Segura, J. J. Hamlin, M. B. Maple, P. Rodriguez-Hernandez and A. Muñoz, *J. Alloys Compd.*, 2014, **587**, 14–20.

